

Lunar detection of ultra-high-energy cosmic rays and neutrinos

J.D. Bray^{*1}, J. Alvarez-Muñiz², S. Buitink³, R.D. Dagkesamanskii⁴, R.D. Ekers⁵, H. Falcke^{3,6}, K.G. Gayley⁷, T. Huege⁸, C.W. James⁹, M. Mevius¹⁰, R.L. Mutel⁷, R.J. Protheroe¹¹, O. Scholten¹⁰, R.E. Spencer¹² and S. ter Veen³

¹Univ. of Southampton; ²Univ. de Santiago de Compostela; ³Radboud Univ. Nijmegen; ⁴Lebedev Physical Institute; ⁵CSIRO ATNF; ⁶ASTRON; ⁷Univ. of Iowa; ⁸KIT; ⁹Univ. of Erlangen-Nuremberg; ¹⁰Univ. of Groningen; ¹¹Univ. of Adelaide; ¹²Univ. of Manchester
E-mail: j.bray@soton.ac.uk

The origin of the most energetic particles in nature, the ultra-high-energy (UHE) cosmic rays, is still a mystery. Due to their extremely low flux, even the 3,000 km² Pierre Auger detector registers only about 30 cosmic rays per year with sufficiently high energy to be used for directional studies. A method to provide a vast increase in collecting area is to use the lunar technique, in which ground-based radio telescopes search for the nanosecond radio flashes produced when a cosmic ray interacts with the Moon's surface. The technique is also sensitive to the associated flux of UHE neutrinos, which are expected from cosmic ray interactions during production and propagation, and the detection of which can also be used to identify the UHE cosmic ray source(s). An additional flux of UHE neutrinos may also be produced in the decays of topological defects from the early Universe.

Observations with existing radio telescopes have shown that this technique is technically feasible, and established the required procedure: the radio signal should be searched for pulses in real time, compensating for ionospheric dispersion and filtering out local radio interference, and candidate events stored for later analysis. For the SKA, this requires the formation of multiple tied-array beams, with high time resolution, covering the Moon, with either SKA-LOW or SKA-MID. With its large collecting area and broad bandwidth, the SKA will be able to detect the known flux of UHE cosmic rays using the visible lunar surface — millions of square km — as the detector, providing sufficient detections of these extremely rare particles to solve the mystery of their origin.

*Advancing Astrophysics with the Square Kilometre Array,
June 8-13, 2014
Giardini Naxos, Sicily, Italy*

*Speaker.

1. Introduction

Cosmic rays are extraterrestrial high-energy particles with a spectrum (Amsler et al. 2008; Gaisser 2006) ranging from around 10^9 eV up to at least 10^{20} eV, at which their origin is unknown. The most energetic, ultra-high-energy (UHE) cosmic rays have an incredible amount of energy for a single particle — comparable to a well-served tennis ball — and it is difficult to explain how they could be produced. The usual mechanism invoked for producing cosmic rays is the acceleration of charged particles by magnetic fields around shocks in the interstellar medium, via the Fermi process. However, the ability of a shock or other region of magnetic turbulence to accelerate a particle up to the highest energies is limited by its ability to keep the particle confined as it accelerates (Hillas 1984), and the observed UHE cosmic rays have energies around the limit achievable by known astrophysical objects such as active galactic nuclei, starburst galaxies, and gamma-ray bursts (Torres & Anchordoqui 2004), suggesting that other mechanisms may need to be invoked to overcome this limit (Protheroe et al. 2003). Alternatively, UHE cosmic rays could originate from the decay of hypothetical supermassive particles, which could either constitute dark matter, or be produced by topological defects such as kinks in cosmic strings formed in the early universe (Berezinsky et al. 2011; Lunardini & Sabancilar 2012). Identifying the source of UHE cosmic rays would improve our understanding of the most extreme astrophysical objects in the universe and the particle acceleration mechanisms they can support, and potentially establish the existence of hitherto-unknown exotic particles.

The study of UHE cosmic rays is difficult because of their extremely low flux: the cosmic ray spectrum follows a power-law of approximately $E^{-2.7}$, and at the highest energies the flux drops so low that less than one particle is detected per km^2 per century. Associating them with specific sources is also difficult because, as charged particles, they are deflected by intervening magnetic fields, so their direction of arrival does not correspond to the direction of their source. Furthermore, at energies exceeding $\sim 6 \times 10^{19}$ eV, they can interact with photons of the cosmic microwave background, either through photopion interactions (for cosmic-ray protons) or photodisintegration (for cosmic-ray nuclei); this GZK effect (Greisen 1966; Zatsepin & Kuzmin 1966) causes attenuation of the cosmic-ray flux at the highest energies, preventing many of them from reaching us. Studies of the few UHE cosmic rays that reach us have found them to be weakly correlated with the distribution of matter in the nearby universe (Abraham et al. 2007), which establishes that they are anisotropic, but the statistics are not sufficient to clearly link them to a specific class of source.

The observations proposed herein explore two major avenues for improving our understanding of the origin of UHE cosmic rays. The first is to observe more cosmic rays of even higher energy. As the energy increases, the magnetic deflection is reduced, and it becomes easier to link a particular cosmic ray with a specific source; together with an increase in the number of detected particles, correlation studies will be greatly improved. Also, the presence or absence of cosmic rays at higher energies will establish whether the observed cutoff in the spectrum (Abraham et al. 2008b; Settimo et al. 2012) is due to the GZK effect, in which case there will be a contribution at higher energies from sources within the GZK horizon; or from an inherent limit on the cosmic-ray energy which can be attained by their sources, in which case the cutoff will be sharp.

The second option is to search for UHE neutrinos, which should be produced both by UHE cosmic ray sources and in GZK interactions. Since neutrinos are uncharged, they travel in straight

lines, and point directly back to their original source. Exotic-particle-decay models for the origin of UHE cosmic rays also predict hard neutrino spectra up to extremely high energies, which would be a clear indication that these models were correct.

Due to the reduced cosmic ray flux at higher energies, and because neutrinos interact only weakly, both these methods require extremely large detectors, significantly greater than even the the 3,000 km² Pierre Auger Observatory (Abraham et al. 2008a) and 700 km² Telescope Array (Abu-Zayyad et al. 2012). The resulting strategy is to remotely monitor a large fraction of the Earth’s surface from a high-altitude balloon (Gorham et al. 2009) or from space (Takahashi et al. 2009). An alternative approach (Dagkesamanskii & Zheleznykh 1989) is to use the Moon as the detector, searching for the radio Askaryan pulse (Askaryan 1962) produced when a UHE cosmic ray or neutrino interacts in the dense lunar regolith. In this manner, a terrestrial radio telescope can use the 19,000,000 km² of visible lunar surface as an UHE particle detector.

Since this idea was proposed, a series of experiments has been conducted by multiple teams with a range of radio telescopes: Parkes (Hankins et al. 1996), Goldstone (Gorham et al. 2004), Kalyazin (Beresnyak et al. 2005), the ATCA (James et al. 2010), Lovell (Spencer et al. 2010), the EVLA (Jaeger et al. 2010), Westerbork (Buitink et al. 2010), Parkes again (Bray 2013), and Parkes and the ATCA in combination (Bray et al. 2011), with preparatory work under way with LOFAR (Singh et al. 2012). These experiments have overcome a range of technical challenges specific to this type of experiment and, together with associated theoretical work, have established the viability of this technique for detecting UHE particles. The increased radio sensitivity possible with the Square Kilometre Array (SKA) will allow Phase 1 to achieve the first lunar-target particle detection, while Phase 2 will provide a ten-fold increase in the detection rate of UHE cosmic rays, and probe new predictions for the UHE neutrino flux, allowing the SKA to address the mystery of the origin of UHE cosmic rays.

2. Particle astronomy with a radio telescope

In this section, we describe the physical mechanism — the Askaryan effect — by which the interaction of high-energy particles produces radio emission, and the methods by which a radio telescope such as the SKA could detect that emission.

2.1 Particle cascades and radio emission

A UHE particle interacting in a dense medium will initiate a particle cascade, with the total energy being distributed over an increasing number of particles as the cascade progresses. Due primarily to entrainment of electrons in the medium, the cascade develops a net negative charge (Askaryan 1962), causing it to radiate coherently at wavelengths greater than the width of the cascade ($\lambda \gtrsim 10$ cm; frequencies up to a few GHz). This radiation is beamed forward as a hollow cone around the cascade axis at the Cherenkov angle ($\sim 55^\circ$), at which it manifests as a single pulse with a duration given by the inverse bandwidth ($\lesssim 1$ ns). The emission is more broadly beamed at lower frequencies, with the radiation pattern extending to perpendicular to the cascade axis (Scholten et al. 2006), and stronger at higher frequencies, as shown in Fig. 1 (left).

If the primary particle is a cosmic ray, then the cascade consists predominantly of hadrons, and develops (in a dense medium such as the lunar regolith) quite quickly, reaching a length of

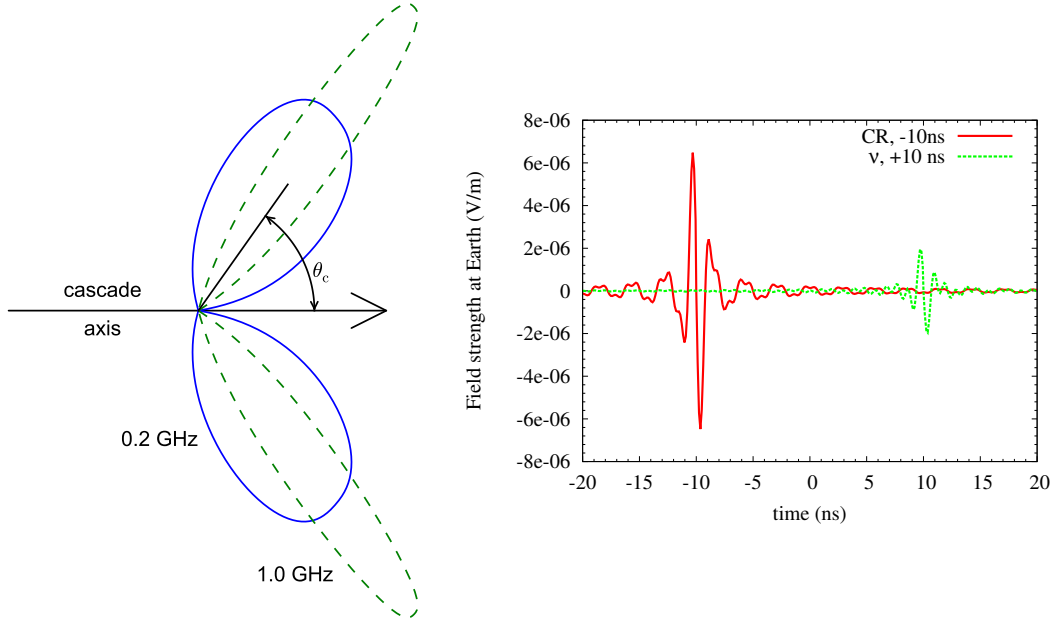


Figure 1: Left: Askaryan emission from a hadronic particle cascade in regolith. The emission is directed forward along the cascade axis as a hollow cone at the Cherenkov angle θ_c . The radiation pattern depends on the frequency, as shown. Right: time-domain pulses (excluding dispersive effects) from 10^{20} eV cosmic ray (CR) and neutrino (ν) interactions with typical geometries, as might be recorded at Earth over a 350 MHz to 1.05 GHz bandwidth.

only ~ 3 m (Alvarez-Muñiz et al. 2006). If the primary particle is a neutrino, it initiates a hadronic cascade carrying $\sim 20\%$ of the primary energy, which behaves in a similar fashion. Depending on the neutrino flavour and interaction type, the remaining energy may go into an electromagnetic cascade, containing only electrons/positrons and photons, but at ultra-high energies these cascades are highly elongated, suppressing their radio emission, and are not generally detectable (James & Protheroe 2009).

A cosmic ray interacts as soon as it enters the regolith, so all such cascades occur close to the lunar surface. At higher frequencies, where the radiation is strongly beamed forward, and refracted further forward as it escapes the lunar surface, the cascade is only detectable if the cosmic ray interacts in a shallow, skimming trajectory, allowing the radiation to escape rather than being directed downward into the Moon. At lower frequencies, where emission sideways from the cascade is coherent (ter Veen et al. 2010), detection is possible over a greater of interaction geometries.

Neutrinos interact less strongly than do cosmic rays, and may occasionally pass through the bulk of the Moon and interact while steeply upgoing relative to the local surface, but at ultra-high energies their interaction cross-section is increased, and they are most likely instead to be detected in a skimming trajectory similar to cosmic rays. They may, however, be well below the lunar surface when they interact, and may be detected at depth up to a few times the radio attenuation length in the lunar regolith (a few tens of metres, depending on frequency). Because many of them will interact too deeply in the Moon to be detected, neutrinos are less likely to be detected than are

cosmic rays (Jeong et al. 2012).

The radiated pulse manifests as a transient bipolar fluctuation in the electric field measured by a radio receiver, as seen in Fig. 1 (right), and confirmed in laboratory measurements at SLAC (see e.g. Miočinović et al. 2006). As the components of the pulse at different frequencies combine coherently in the voltage domain, the signal-to-noise ratio in power scales linearly with bandwidth, in contrast to the square-root law typical in other fields of radio astronomy. The sensitivity of a radio telescope defines a minimum detectable pulse amplitude, which in turn defines a minimum detectable particle energy; the SKA, with its superior sensitivity, will probe down to lower particle energies than has previously been possible with this technique. As the pulse has an increasing spectrum, up to a turnover at a few GHz or below due to either decoherence or absorption, observations aiming to minimise the detection threshold tend to favour higher frequencies. Above the threshold energy, the sensitivity of an experiment to a particle flux is defined by the geometric aperture, with units of area times solid angle. The radio pulse at low frequencies is more broadly beamed, covering a larger solid angle, which favours lower frequencies for observations significantly above the detection threshold. For neutrinos, low frequencies also allow a cascade to be detected deeper in the regolith, as the radio attenuation length is lower, which increases the detector volume and hence further increases the aperture.

This complex dependence of sensitivity on frequency means that both SKA1-LOW and SKA1-MID are useful and complementary in this role, and explore different regions of the energy-flux phase space. (SKA1-SUR, despite its larger field of view, offers no advantage over SKA1-MID, as the field of view of the latter is sufficient to see the entire Moon.) The discussion below, except where noted, applies to both instruments.

2.2 Observational requirements

The observational requirements for detecting a nanosecond-scale pulse from the Moon are different from those of other areas of radio astronomy. Such a short pulse is only detectable in the original time-domain voltages sampled by the receiver, at their full native time resolution. Storing this quantity of data is usually impractical, so it is generally necessary to maintain a buffer of data and search for a pulse in real time, triggering the storage of the buffer only when a candidate event is found; the proposed signal path is shown in Fig. 2. The trigger criteria need not be perfectly optimised in real time, but they must be good enough that any plausible events are stored so that they can be analysed retrospectively.

As an array, the SKA is only fully sensitive to a transient signal when it is combined to form a tied-array beam. Buffered data can (and should) be kept from individual dishes/stations of the SKA so that they can be combined retrospectively, but for triggering purposes it is necessary to form beams with at least the core of the array in real time, to have sufficient sensitivity to detect candidate events. The specifications for SKA1-MID include such a beamformer (Dewdney 2013), and a similar feature for SKA1-LOW has been proposed. The SKA1-MID beamformer, for bands 1 and 2, will have the capacity to form sufficient beams to tile across the visible surface of the Moon ($\sim 0.2 \text{ deg}^2$), and to tile in frequency to cover the entire band.

For a nanosecond-scale pulse to be detected, the signal for each beam should consist of a single sequence of voltage samples, with inverse-bandwidth time resolution, so that a pulse — which might comprise a single high-amplitude sample — can be identified. This presents a problem,

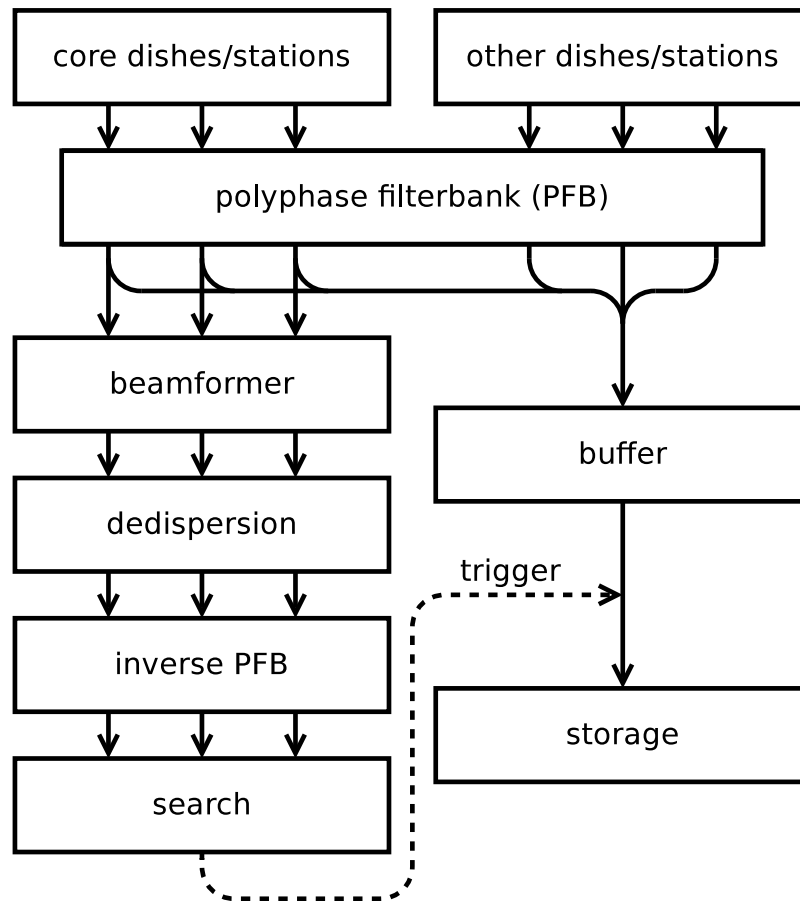


Figure 2: Proposed signal path as described in Sec. 2. The signals from the core dishes (SKA-MID) or stations (SKA-LOW) are, after being channelised by the polyphase filterbank, formed into sufficient beams to tile across the visible surface of the Moon. While still channelised, they are dedispersed to compensate for the effects of the ionosphere, and then converted back to pure time-domain signals by an inverse polyphase filterbank. The resulting signals are then searched for a nanosecond-scale pulse meeting several RFI-rejection criteria. If one is found, it is used to trigger the storage of buffered data from all dishes/stations, which can be retrospectively processed to analyse the pulse with the full sensitivity of the entire array.

as the beamformer acts on the signal after it has passed through a polyphase filterbank, which separates it into frequency channels with inverse-channelwidth time resolution. Fortunately, it is possible to invert a polyphase filterbank to restore the time-domain signal for each beam, with a minor loss of efficiency (Singh et al. 2012).

A lunar-origin nanosecond-scale radio pulse is dispersed as it passes through the ionosphere. The degree of dispersion is minor compared to that for interstellar signals but, due to the extremely short pulse, it still causes a significant loss of amplitude, and must be corrected. Because the signal is channelised during the beamforming stage, it is relatively simple to dedisperse it by applying an appropriate phase factor, but it may be necessary to test the signal for a trigger condition at multiple dispersion measures, depending on how precisely the dispersion can be predicted. Current techniques are based on ionosonde measurements or GPS-based global electron content maps;

improvements are possible through direct measurements of dispersion to GPS satellites from a ground station at the telescope site (currently on trial at Parkes) or through measurements of the Faraday rotation of polarised thermal emission from the Moon itself (McFadden et al. 2011).

As transient detection experiments aim to detect single, unrepeated events, they are highly susceptible to radio-frequency interference (RFI): it is necessary to reliably exclude every single instance of nanosecond-scale impulsive RFI to be certain that any remaining events are true lunar-origin Askaryan pulses. The simplest way to achieve this is to require a coincident detection on multiple independent antennas (e.g. Gorham et al. 2004), but this limits the sensitivity of the experiment. In experiments which have used the full coherent sensitivity of a telescope’s entire collecting area, the most effective technique is to exclude pulses that are detected with multiple beams directed at different parts of the Moon, as employed with the WSRT (Buitink et al. 2010) and the Parkes telescope (Bray 2013). In the latter case, RFI was successfully excluded with high fidelity in real time, and completely in retrospective processing. The SKA will have the further advantages of a less active RFI environment and a greater number of beams on the Moon, and we are confident that RFI triggers can be excluded with sufficient reliability that they will not dominate the real-time trigger rate, and those which do cause a trigger can be eliminated in retrospective processing.

If RFI is excluded, then the trigger rate will be dominated by thermal fluctuations in the voltage. As each trigger causes the current contents of the buffers to be stored to disk, the speed with which these data can be stored will determine the supportable trigger rate, and hence how low the trigger threshold can be set. Assuming a trigger condition of a global OR over all the on-Moon beams, so that a pulse can be detected from anywhere on the Moon, a trigger threshold of $\sim 7\sigma$ (relative to the thermal noise) would suffice to keep the background trigger rate around 1 Hz. Assuming a buffer length of $10 \mu\text{s}$, primarily to assist in characterising RFI, and 8-bit sampling, this results in a manageable data-storage rate of $\sim 10 \text{ MB/s}$. This value applies to both SKA1-LOW and SKA1-MID: the former has more stations and the latter has a higher sampling rate, but these effects approximately cancel out.

Retrospective analysis will achieve greater sensitivity than the real-time beams, due to the use of the entire array rather than just the beamformed core, resynthesising the beam directly on the source position, more precise dedispersion, etc. These effects are typically of the order of a few tens of percent. Combined, they might allow retrospective analysis to reach a sensitivity $\sim 2\times$ that available in real time; i.e. the real-time sensitivity would be worse than the theoretical sensitivity by a factor of 2, or $\sqrt{2}$ in the voltage domain. This means that a 7σ threshold in the real-time trigger would ensure that any pulse exceeding $7\sqrt{2}\sigma \sim 10\sigma$ with the full theoretical sensitivity would be stored and detected. We use this 10σ threshold when calculating the sensitivity in Sec. 3. At this level, the false detection rate is less than one per century.

Apart from their scientific potential, experiments of this type have historically also been useful as instrumental debugging aids. The first LUNASKA experiment with the ATCA used precision timing of nanosecond-scale transient RFI events to locate their sources to within a few metres (James 2009). An experiment with the VLA identified a linearity problem in the receivers (Jaeger et al. 2010); an experiment with the Parkes radio telescope identified a similar problem and corrected it (Bray 2013). A further experiment with the ATCA (Bray et al. 2011) led to the development of a highly-effective system for excising microsecond-scale pulsed RFI using the raw time-series data.

2.3 Preferred band

The nature of the emission discussed above indicates that, during SKA Phase 1, the SKA1-MID bands would be useful for making the first detections of UHE cosmic rays with this technique, since their higher frequencies will compensate for their lower effective area; but that for Phase 2, SKA1-LOW band 1 would provide both the highest rate of UHE cosmic-ray detections, and be the most sensitive to models of the UHE neutrino flux. While we expect this result to hold in the future, the relative utility of the SKA bands may change, due both to uncertainties in the effects of lunar surface roughness — particularly for high-frequency observations of cosmic rays — and for technical reasons as the designs of the instruments mature, particularly with respect to the availability of beamforming capacity. Therefore, while we expect the SKA1-LOW band of 100–250 MHz to be the instrument of choice for utilising the lunar Askaryan technique with the SKA, we also include expectations for the other bands.

2.4 Direction and energy resolution

The proportionality of the low-frequency signal strength in Askaryan pulses to cascade energy will allow a determination of the primary particle energy, particularly for cosmic ray interactions where the entire primary energy is deposited as a hadronic cascade, and absorption effects in the lunar regolith are negligible. Such absorption features will also allow neutrino interactions to be identified, although the primary spectrum of these particles will have to be determined by deconvolving the observed pulse spectrum, due to the random inelasticity of their interactions.

The polarisation of Askaryan signals — which is always in the cascade-observer plane — combined with the strong dependence of the signal strength as well as the frequency spectrum on the interaction geometry, will allow the arrival directions of primary particles to be determined. While the resolution on particle direction is not expected to be as good as with terrestrial detectors (James et al. 2008), the utility of directional resolution is limited to the intrinsic angular dependence in the UHE particle flux, which varies only over large angular scales (Abraham et al. 2008a). In particular, the achievable angular resolution will be more than sufficient to study nearby UHE cosmic ray candidates such as Centaurus A, which is tentatively associated with a number of UHE cosmic rays observed the the Pierre Auger Observatory on scales of order 20° (Abreu et al. 2011).

3. SKA performance

Simulations of the SKA sensitivity to UHE particles using the lunar Askaryan technique were performed by a detailed Monte Carlo code (James & Protheroe 2009). This code simulates particle propagation and interactions in the Moon, radio-wave production according to Alvarez-Muñiz et al. (2006), its subsequent absorption in and transmission through lunar rock, and signal detection based upon an assumed instrumental sensitivity and the calculated pulse strength. The accuracy of this simulation has been verified by comparisons with (semi-)analytic calculations in limiting cases (Gayley et al. 2009; Scholten et al. 2006).

The dominant uncertainties in the simulation are the interaction cross-sections for UHE neutrinos and the effects of lunar surface roughness. The former have an uncertainty at 10^{20} eV of $\sim 20\%$ within the standard model (Cooper-Sarkar et al. 2011), and exotic extra-dimensional models suggest that they could be larger by 1–2 orders of magnitude (Connolly et al. 2011); we use the

Band	f_{\min} (MHz)	f_{\max} (MHz)	Phase 1		Phase 2	
			$(A_{\text{eff}}/T_{\text{beam}})$ m^2/K	E_{thresh} $\text{V}/\text{m}/\text{MHz}$	$(A_{\text{eff}}/T_{\text{beam}})$ m^2/K	E_{thresh} $\text{V}/\text{m}/\text{MHz}$
LOW 1	100	350	1000	1.4×10^{-9}	4000	7.2×10^{-10}
LOW 2	350	700	1000	1.2×10^{-9}	4000	6.0×10^{-10}
MID 1	350	1050	143	2.3×10^{-9}	844	9.4×10^{-10}
MID 2	950	1760	143	2.1×10^{-9}	844	8.7×10^{-10}

Table 1: Estimated sensitivities ($(A_{\text{eff}}/T_{\text{beam}})$, including lunar thermal emission) and signal detection threshold thresholds ($\text{V}/\text{m}/\text{MHz}$) for SKA observation bands. SKA-MID Phase 1 treats both 64 MEERKAT and 190 SKA antennas identically, while SKA-MID Phase 2 uses 1500 SKA antennas.

standard-model cross-sections of Gandhi et al. (1998). For the latter, we use the self-affine surface model of Shepard et al. (1995), implementing it by randomly deviating the lunar surface on length scales corresponding to the characteristic size of the radiation transmission region on the surface.

Due to the broadband nature of the signal, the optimal frequency range for lunar observations with the SKA can only be determined by simulating all frequency bands up to the highest-frequency band for which beamforming across the entire Moon is practical. We therefore consider the SKA-LOW band and its potential second Nyquist band (SKA-LOW 1 and 2), as well as the two lowest-frequency receivers for SKA-MID (SKA-MID 1 and 2). As described in Sec. 2, the sensitivity of these SKA bands to lunar signals must be calculated relative to the lunar thermal emission which, at approximately 225 K (Troitskij & Tikhonova 1970), is brighter than the sky at frequencies above approximately 168 MHz. Averaged over the SKA-LOW band, both the lunar emission and the sky background will have similar strengths, so the SKA-LOW sensitivity from Dewdney (2013) is used unchanged (although this is likely optimistic for the second Nyquist band, SKA-LOW 2). In the case of SKA-MID, the lunar emission will dominate, and is added to the system temperature. The resulting sensitivities are given in Table 1, where the signal detection thresholds correspond to 10 times the effective beam root-mean-square noise voltage. Using these thresholds, the effective areas, expected limits, and event rates for each band were calculated, assuming that the observational requirements — dedispersion, triggering, RFI discrimination etc. — had been satisfied.

3.1 Cosmic rays

The effective geometric aperture to cosmic rays, with dimensions of area times solid angle, is given in Fig. 3 (left). In general, the minimum detectable cosmic-ray energy decreases with increasing frequency, while the high-energy aperture increases at lower frequencies. While all studied bands will be sensitive to the flux at 56 EeV and above, at lower energies only SKA-LOW 2 will exhibit a greater aperture than the Pierre Auger Observatory (PAO) in Phase 1; for Phase 2, SKA-LOW 1 and SKA-MID 1 will also have a greater aperture than PAO in this range. Convolved with the (rapidly-decreasing) model cosmic ray spectrum from Abraham et al. (2010), the event rates are shown as a function of cosmic-ray energy in Fig. 3 (right); the total yearly event rates are given in Table 2.

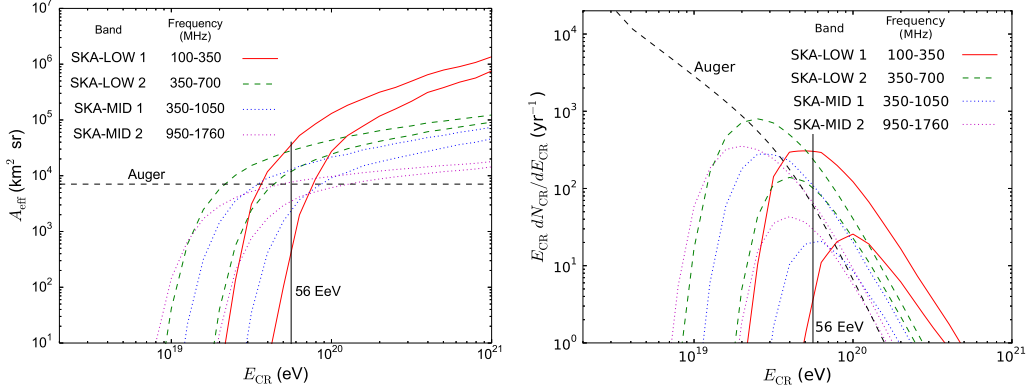


Figure 3: SKA effective apertures to (left), and detection rates of (right), UHE cosmic rays: in each case, SKA Phase 1 is given by the bottom lines, and Phase 2 by the top. Estimates for SKA-LOW and SKA-MID are presented, indicating the frequency range of each band. Apertures and rates of the Pierre Auger Observatory (‘Auger’) are also shown, as is the 56 EeV threshold used in the Auger anisotropy analysis (Abraham et al. 2007).

SKA Band	Phase 1		Phase 2	
	$E_{CR} > 56$ EeV	All	$E_{CR} > 56$ EeV	All
LOW 1	22	23	165	335
LOW 2	37	132	74	904
MID 1	11	18	36	298
MID 2	10	40	18	407
Auger	15 ($E_{CR} > 56$ EeV)			

Table 2: Expected detection rates N_{CR} (CR yr⁻¹) for the simulated SKA bands and phases shown in Table 1, compared to the rate at which the Pierre Auger Observatory detects events above 56 EeV.

Fig. 3 (right) shows that for Phase 2 of the SKA, SKA-LOW 1 will give the greatest rate of UHE cosmic-ray detections in the $E_{CR} > 56$ EeV range, at approximately 165 yr⁻¹, which is 11 times the PAO rate of approximately 15 such events per year, and equivalent to a ground array covering 33,000 km² — an area larger than Belgium. Since the SKA-LOW 1 aperture increases rapidly with energy, such a sample of events will be biased towards those with higher energy, and therefore will represent a relatively better sample for determining the cosmic ray origin than even these numbers would suggest.

The goal for Phase 1 of the SKA however would not be statistics above 56 EeV, but rather verification of the technique, for which cosmic rays of any energy would do. For this purpose, SKA-LOW 2 would expect 132 events yr⁻¹, allowing a reasonable sample of 11 events to be collected with one month’s observation time. If SKA-LOW 2 is not available, then the the SKA-MID bands at progressively higher frequencies would be better-suited to such observations, with expected rates of 18 events of all energies per year for SKA-MID 1, and 40 events for SKA-MID 2.

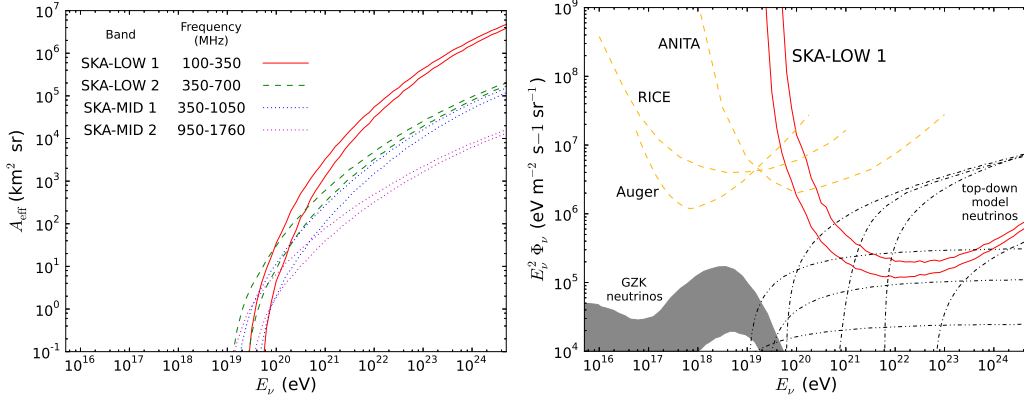


Figure 4: (left) SKA effective apertures to UHE neutrinos; and (right) expected limits from a 1,000 hr observation on the UHE neutrino flux. The SKA Phase 1 (2) apertures are given by the bottom (top) lines, while the Phase 1 (2) limits are given by the top (bottom) lines. Predictions are given for the neutrino flux from GZK interactions (Allard et al. 2006) and from top-down CR origin models (Berezinsky et al. 2011; Lunardini & Sabancilar 2012). Limits set by competing experiments Auger (Abreu et al. 2013), RICE (Kravchenko et al. 2012) and ANITA (Gorham et al. 2010, 2012) are also shown.

3.2 Neutrinos

The effective geometric apertures to neutrinos are shown in Fig. 4 (left) — the behaviour is similar to that for cosmic rays. The choice of frequency range — which also determines the depth at which neutrino interactions may be observed — is the main factor which determines the aperture above 3×10^{20} eV, where SKA-LOW 1 dominates in both Phase 1 and Phase 2. Below 10^{20} eV, the sensitivity of the instrument is the main factor, with the aperture of SKA-LOW 2 being highest.

The expected limits on the UHE neutrino flux from 1,000 hr of SKA observations are compared to current limits (from dedicated detectors, with observation times of years) in Fig. 4 (right), and expectations on the flux. The SKA could significantly improve on current limits in the extremely energetic range above 10^{20} eV, where SKA-LOW 1 would provide the strongest tests of UHE neutrino flux predictions such as those of Lunardini & Sabancilar (2012) and Berezinsky et al. (2011).

3.3 Effects of changing performance

The expected sensitivities calculated above assume full SKA performance. There are three main ways in which the assumed sensitivity of the SKA might not be reached — by a reduced beamforming capability, so that only a fraction of the Moon can be observed; the inability to buffer data from telescopes/stations which do not form part of the real-time beamforming, so that their sensitivity can not be added post-trigger; and from a simple reduction in the total size or bandwidth of the SKA. In order to estimate the likely effects of such a reduction — and to estimate what science goals might be achieved when the SKA is still only partially built — the simulations above were repeated for a reduction in sensitivity of 50%. This corresponds to a decrease of 50% in either the effective area or the bandwidth, in contrast to conventional radio observations, for which the sensitivity only has a square-root dependence on the bandwidth.

The effect on the performance of the SKA for setting limits on the UHE neutrino flux is small, since in the UHE regime where the SKA could set new, stronger limits, the raw observation time matters more than sensitivity. The effect on the cosmic ray sensitivity is strong however, since even for the full SKA Phase 2, the detection threshold for SKA-LOW 1 is not much below 56 EeV (see Fig. 3). A 25% (50%) decrease in sensitivity for SKA-LOW would reduce the number of detected $E_{\text{CR}} > 56$ EeV events per year from 165 to 120 (72), requiring a proportionally greater observation time to achieve the required statistics. Additionally, the goal of observing the cosmic ray flux with Phase 1 becomes much more difficult, with a 50% reduction in sensitivity leading to cosmic ray rates for SKA-MID receivers 1 and 2 of 5 and 13 respectively (compared with 18 and 40 for the full sensitivity).

4. Conclusion

The origin of the highest-energy particles in nature, the UHE cosmic rays, is still unknown. Using the lunar Askaryan technique, the SKA will have the capability to observe UHE cosmic rays at a rate of more than ten times that of the largest current observatory, the 3,000 km² Pierre Auger Observatory in Argentina. The SKA will also be able to detect, or place strong limits on, the flux of their as-yet unobserved counterparts, the UHE neutrinos, which are predicted both from the cosmic ray production mechanism, and from interactions during their propagation.

Observations of these extremely rare particles will allow a new understanding of their source(s), thought to be the most extreme and exotic objects in the universe — the jets and/or lobes of active galactic nuclei, gamma-ray bursts, or even the decay of exotic supermassive particles. Initial observations with Phase 1 of the SKA, with either SKA1-MID or the proposed second Nyquist band of SKA1-LOW, will provide the first detections, and enable a longer dedicated observation in the 100–350 MHz band with SKA-LOW during Phase 2.

The lunar Askaryan technique is a unique observing mode, and has its own technical requirements. In particular, the ability to form coherent beams over the entire lunar disc at full time resolution is crucial, as is the ability to record pre-beamformed data from each station in order to exclude terrestrial RFI. The necessary techniques to overcome these challenges have already been developed at Parkes, Goldstone, Kalyazin, the ATCA, Lovell, the EVLA, Westerbork and LOFAR. Applied to the SKA, they will enable an order-of-magnitude improvement in our ability to study the most extreme particles in the universe.

References

- J. Abraham et al. (Pierre Auger Coll.) 2007, *Science*, 318, 938
- J. Abraham et al. (Pierre Auger Coll.) 2008a, *Astropart. Phys.*, 29, 188
- J. Abraham et al. (Pierre Auger Coll.) 2008b, *Phys. Rev. Lett.*, 101, 061101
- J. Abraham et al. (Pierre Auger Coll.) 2010, *Phys. Lett. B*, 685, 239
- P. Abreu et al. (Pierre Auger Coll.) 2011, *JCAP*, 6, 22

- P. Abreu et al. (Pierre Auger Coll.) 2013, Proc. 33rd ICRC, Rio de Janeiro
- T. Abu-Zayyad et al. (Telescope Array Coll.) 2012, ApJ, 757, 26
- D. Allard, M. Ave, N. Busca et al. 2006, JCAP, 9, 005
- J. Alvarez-Muñiz, E. Marqués, R.A. Vázquez & E. Zas 2006, Phys. Rev. D, 74, 023007
- C. AMSLER et al. 2008, Phys. Lett., B667, 1
- G.A. Askaryan 1962, Sov. Phys. JETP, 14, 441
- A.R. Beresnyak, R.D. Dagkesamanskii, I.M. Zheleznykh et al. 2005, Astron. Rep., 49, 127
- V. Berezhinsky, E. Sabancilar & A. Vilenkin 2011, Phys. Rev. D, 84, 085006
- J.D. Bray, R.D. Ekers, C.W. James et al. 2011, Proc. 32nd ICRC, Beijing
- J.D. Bray 2013, PhD thesis, University of Adelaide
- S. Buitink, O. Scholten, J. Bacelar, R. Braun, A.G. de Bruyn et al. 2010, A&A, 521, A47
- A. Connolly, R.S. Thorne & D. Waters 2011, Phys. Rev. D, 83, 113009
- A. Cooper-Sarkar, P. Mertsch & S. Sarkar 2011, JHEP, 2011, 42
- R.D. Dagkesamanskii & I.M. Zheleznykh 1989, Sov. Phys. JETP Lett., 50, 259
- P.E. Dewdney 2013, SKA1 System Baseline Design
- T.K. Gaisser 2006, J. Phys.: Conf. Ser., 47, 15
- K.G. Gayley, R.L. Mutel & T.R. Jaeger 2009, ApJ, 706, 1556
- R. Gandhi, C. Quigg, M.H. Reno & I. Sarcevic 1998, Phys. Rev. D, 58, 039009
- P.W. Gorham, C.L. Hebert, K.M. Liewer et al. 2004, Phys. Rev. Lett., 93, 041101
- P.W. Gorham et al. (ANITA Coll.) 2009, Astropart. Phys., 32, 10
- P.W. Gorham et al. (ANITA Coll.) 2010, Phys. Rev. D, 82, 022004
- P.W. Gorham et al. (ANITA Coll.) 2012, Phys. Rev. D, 85, 049901
- K. Greisen 1966, Phys. Rev. Lett., 16, 748
- T.H. Hankins, R.D. Ekers & J.D. O'Sullivan 1996, MNRAS, 283, 1027
- A.M. Hillas 1984, Ann. Rev. Astron. Astrophys., 22, 425
- T.R. Jaeger, R.L. Mutel & K.G. Gayley 2010, Astropart. Phys., 43, 293
- C.W. James 2009, PhD thesis, University of Adelaide

- C.W. James, R.D. Ekers, R.A. McFadden & R.J. Protheroe 2008, Proc. 30th ICRC, Merida
- C.W. James, R.D. Ekers, J. Alvarez-Muñiz et al. 2010, Phys. Rev. D, 81, 042003
- C.W. James & R.J. Protheroe 2009, Astropart. Phys., 30, 318
- Y.S. Jeong, M.H. Reno & I. Sarcevic 2012, Astropart. Phys., 35, 383
- I. Kravchenko, S. Hussain, D. Seckel et al. 2012, Phys. Rev. D, 85, 062004
- C. Lunardini & E. Sabancilar 2012, Phys. Rev. D, 86, 085008
- R.A. McFadden, R.D. Ekers & J.D. Bray 2011, Proc. 32nd ICRC, Beijing
- P. Miočinović, R.C. Field, P.W. Gorham et al. 2006, Phys. Rev. D, 74, 043002
- R.J. Protheroe, A.-C. Donea & A. Reimer 2003, Astropart. Phys., 19, 559
- O. Scholten, J. Bacelar, R. Braun et al. 2006, Astropart. Phys, 26, 219
- M. Settimo et al. (Pierre Auger Coll.) 2012, Eur. Phys. J. Plus, 127, 87
- M.K. Shepard, R.A. Brackett & R.E. Arvidson 1995, J. Geophys. Res., 100, 11709
- K. Singh, M. Mevius, O. Scholten et al. (LOFAR Coll.) 2012, NIMA, 664, 171
- R.E. Spencer, A. Macfarlane, O. Mills & L. Piccirillo 2010, Proc. 10th EVN Symposium, 097
- Y. Takahashi et al. (JEM-EUSO Coll.) 2009, New J. Phys., 11, 065009
- S. ter Veen, S. Buitink, H. Falcke et al. 2010, Phys. Rev. D, 82, 103014
- D.F. Torres & L.A. Anchordoqui 2004, Rep. Prog. Phys., 67, 1663
- V.S. Troitskij & T.V. Tikhonova 1970, Izv. Vyssh. Uchebn. Zaved. Radiofiz., 13, 1272
- G. Zatsepin & V. Kuzmin 1966, Pis'ma Zh. Eksp. Teor. Fiz., 4, 114